SUPPORTING METEOROLOGICAL FIELD EXPERIMENT MISSIONS AND POSTMISSION ANALYSIS WITH SATELLITE DIGITAL DATA AND PRODUCTS

BY JEFFREY HAWKINS AND CHRISTOPHER VELDEN

Digital satellite remote-sensing imagery and derived products can greatly aid field project success in terms of both real-time logistics and supporting scientific hypotheses.

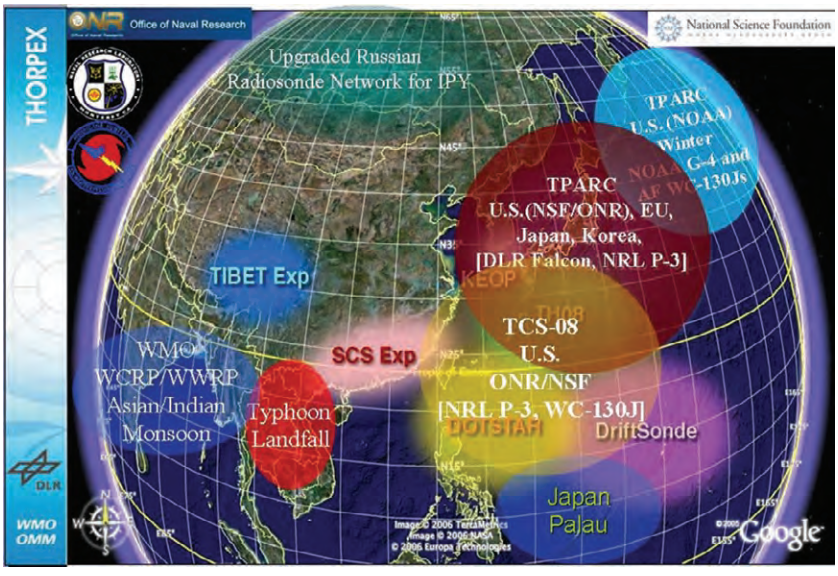

FIG. 1. Schematic of the T-PARC field program elements and coverage, including the TCS-08 TC structure project (courtesy: Pat Harr, NPS and David Parsons, University of Oklahoma).

In this paper we focus on a good recent example of how multiple satellite-based datasets and products played an important role in supporting a meteorological field experiment: the Tropical Cyclone Structure 2008 (TCS-08) project, part of the much larger The Observing System Research and Predictability Experiment (THORPEX) Pacific Regional Area Campaign (T-PARC) field program, was designed to study tropical cyclones (TCs) in the western North Pacific domain during August and September 2008. The field program (Fig. 1) involved international collaborators and leveraged a special suite of observing resources, including ▶

Report Documentation Page

Form Approved
OMB No. 0704-0188

1. REPORT DATE	2. REPORT TYPE	3. DATES COVERED
APR 2011		**00-00-2011 to 00-00-2011**

4. TITLE AND SUBTITLE	5a. CONTRACT NUMBER
Supporting Meteorological Field Experiment Missions and Postmission Analysis with Satellite Digital Data and Products	5b. GRANT NUMBER
	5c. PROGRAM ELEMENT NUMBER
6. AUTHOR(S)	5d. PROJECT NUMBER
	5e. TASK NUMBER
	5f. WORK UNIT NUMBER
7. PERFORMING ORGANIZATION NAME(S) AND ADDRESS(ES) **Naval Research Laboratory,Marine Meteorology Division,7 Grace Hopper Ave., MS#2,Monterey,CA,93923**	8. PERFORMING ORGANIZATION REPORT NUMBER
9. SPONSORING/MONITORING AGENCY NAME(S) AND ADDRESS(ES)	10. SPONSOR/MONITOR'S ACRONYM(S)
	11. SPONSOR/MONITOR'S REPORT NUMBER(S)

12. DISTRIBUTION/AVAILABILITY STATEMENT
Approved for public release; distribution unlimited

13. SUPPLEMENTARY NOTES

14. ABSTRACT

15. SUBJECT TERMS

16. SECURITY CLASSIFICATION OF:			17. LIMITATION OF ABSTRACT	18. NUMBER OF PAGES	19a. NAME OF RESPONSIBLE PERSON
a. REPORT **unclassified**	b. ABSTRACT **unclassified**	c. THIS PAGE **unclassified**	**Same as Report (SAR)**	**14**	

aircraft, ships, buoys, radiosondes, driftsondes, dropsondes, and more. TCS-08 was sponsored by the U.S. Office of Naval Research (ONR) and focused on detailed atmospheric measurements of TC genesis, inner core structure, and extratropical transitions (ETs) to better understand intensity changes while also sampling the ocean response to TC passages.

In T-PARC/TCS-08, a suite of geostationary (GEO) and low-earth-orbiting (LEO) sensors were employed to help guide daily mission planning, forecasts, and outlooks, and also to enhance postmission analysis studies. This paper chronicles the T-PARC/TCS-08 project's satellite-observing tools, imagery, and derived products that provided real-time guidance and postmission analysis information. We synthesize those that were critical to T-PARC/TCS-08 as an example of how satellite-based remote sensing can be optimized to provide dedicated field campaign support.

REAL-TIME MISSION PLANNING, NOWCASTING, AND FORECAST SUPPORT.

Daily decision making on flight planning for aircraft assets involves an intricate assessment of the evolving meteorology, project goals, crew rest, and asset inventories. For T-PARC/TCS-08, the aircraft included an Air Force WC-130J "hurricane hunter" and a Naval Research Laboratory (NRL) WP-3D (both based in Guam) and two higher-altitude jet aircraft. All aircraft conducted TC reconnaissance and surveillance missions to gather crucial in situ and in some cases remotely sensed observations. The mission planning involved forecast support in advance of the intensive observing period and nowcasting support during the aircraft surveillance flights. Daily operations center Webcast briefings hosted by the Naval Postgraduate School (NPS, in Monterey, California) provided the "big picture" analysis and outlook for potential systems of interest, or "invests."

A suite of satellite imagery and tailored products formed an integral part of these briefings and set the stage for principal investigator decision making regarding potential missions. Real-time imagery and derived products covering synoptic and "storm centric" areas were routinely created and made available to the operations center through dedicated Web sites (described later in the text).

Geostationary satellite data. The primary source for high-temporal-resolution satellite data was the Japanese Meteorological Agency's (JMA) *Multifunctional Transport Satellite (MTSAT)-1R* geostationary satellite. Digital visible (VIS), infrared (IR), and water vapor (WV) images were routinely provided at half-hourly intervals. These images were collected on the University of Wisconsin—Madison's Cooperative Institute for Meteorological Satellite Studies (CIMSS) mass storage system and disseminated to the National Center for Atmospheric Research (NCAR) Earth Observing Laboratory (EOL) T-PARC field catalog for final archive and future scientific studies.

The *MTSAT-1R* multispectral imager data were processed hourly in real time to extract atmospheric motion vectors (AMVs) by following cloud and/or water vapor targets between sequential (30 min) images using automated tracking and quality control algorithms developed at CIMSS (Velden et al. 2005). These AMVs were crucial in providing detailed evolving flow characteristics during T-PARC/TCS-08 events. Kinematic diagnostics and their evolution, such as low-level convergence, upper-level divergence, and deep-layer mean shear, were consistently relied on in mission planning.

In addition to the routine hourly AMV fields, supplemental rapid-scan (RS) operations were conducted by JMA using *MTSAT-2R* (spare satellite) during select periods. The RS imaging cycle (per every hour) consisted of three 15-min Northern Hemisphere (NH) images, then three 4-min limited-area images or two 7-min limited-area images in succession. RS AMV datasets were postprocessed by CIMSS for research-quality reanalyses. Figure 2 illustrates the enhancement to the AMV datasets when 15-min and 4-min RS images were available. Note the increased spatial coverage of the RS AMVs that enables the capture of details in the TC and near-environmental flow fields. All of the CIMSS AMV datasets are available from the EOL T-PARC data catalog archive.

The MTSAT digital imagery was also used to generate other TC-specific products for real-time use, including high-priority storm intensity estimates. The well-known Dvorak technique is based on the principles of satellite imagery cloud pattern recognition, with the amount of organization directly correlated

AFFILIATIONS: Hawkins—Marine Meteorology Division, Naval Research Laboratory, Monterey, California; Velden—Cooperative Institute for Meteorological Satellite Studies, Madison, Wisconsin
CORRESPONDING AUTHOR: Jeffrey Hawkins, Naval Research Laboratory, 7 Grace Hopper Ave., MS#2, Monterey, CA 93923
E-mail: jeffrey.hawkins@nrlmry.navy.mil

The abstract for this article can be found in this issue, following the table of contents.
DOI:10.1175/2011BAMS3138.1

In final form 9 April 2011

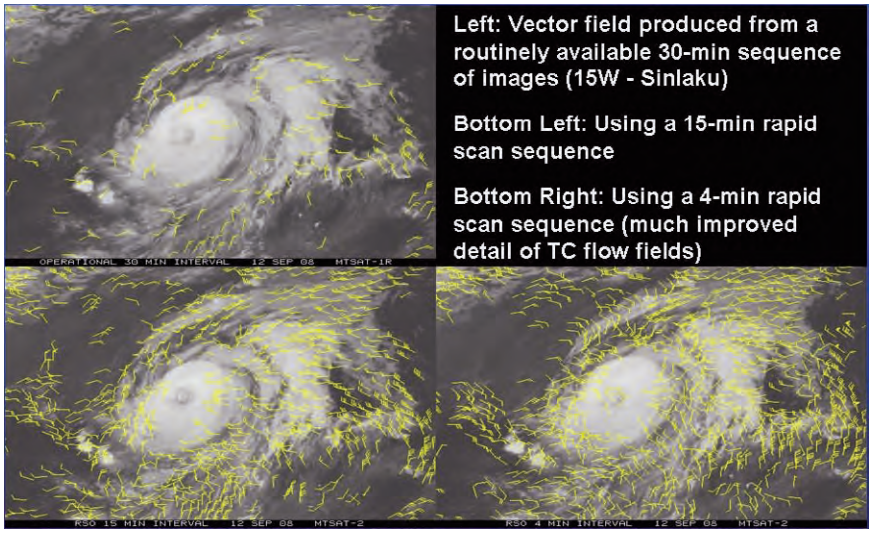

Fig. 2. *MTSAT-2* AMVs from 1200 UTC 12 Sep 2008 derived using (top left) 30-, (bottom left) 15-, and (bottom right) 4-min interval RS imagery, overlain on corresponding IR imagery of Typhoon Sinlaku during T-PARC/TCS-08.

to TC intensity. Trained satellite analysts can subjectively determine the cloud pattern type and in some cases use actual brightness temperatures (T_B) to relate specific characteristics to storm development stages, or Dvorak "T" (tropical) numbers [see Velden et al. (2006) for further details]. More recently, scientists collaborated to automate the Dvorak technique, resulting in an algorithm referred to as the advanced Dvorak technique (ADT) (Velden et al. 1998; Olander and Velden 2007). The ADT was designed to minimize the time-consuming process of cloud pattern typing and the human subjectivity in the method's rules application stages. This algorithm operates on GEO satellite IR imagery and is competitive with subjective applications. During T-PARC/TCS-08, near-real-time ADT estimates were routinely available and used extensively by operations center nowcasters (see Fig. 3 for an example).

LEO satellite data. LEO satellite sensors provide spectral and spatial capabilities not available on GEO platforms and were critical to the science and T-PARC/TCS-08 field program mission goals. In particular, multichannel passive and active microwave imagers/sounders and radars use different parts of the electromagnetic spectrum from the VIS/IR imagers to extract environmental measurements and derived parameters. The LEO data were collected, processed, distributed, and archived by the NRL and made available to the EOL field catalog.

Passive microwave imagers. Passive microwave digital imagery and derived products have significantly benefited the global TC monitoring effort (Hawkins et al. 2001, 2009). The "ice-scattering channels" on most microwave imagers (85–91 GHz) are particularly adept at isolating TC rainband and eyewall structural features. Intense convection dramatically lowers the equivalent blackbody T_B caused by scattering from precipitation-size ice hydrometeors. Fortunately, TC cirrus canopies, which often shield organized cloud structure in VIS/IR

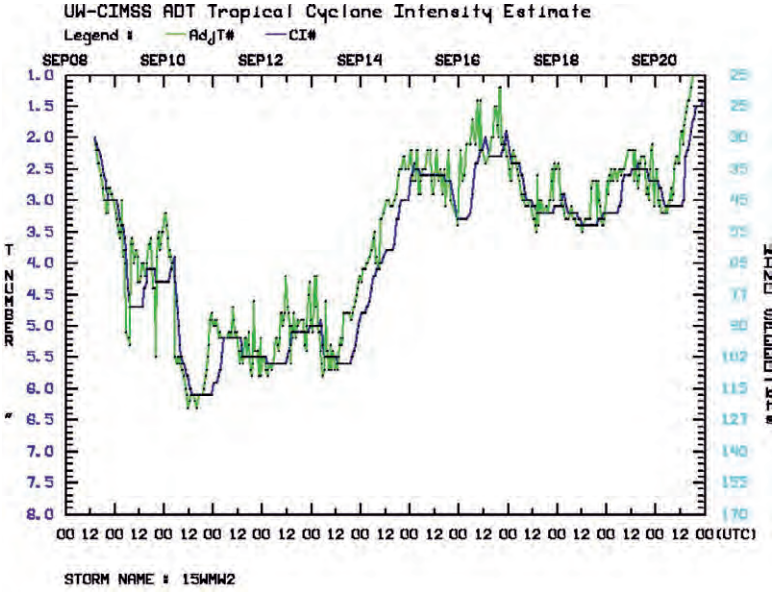

Fig. 3. Example of the ADT output for Typhoon Sinlaku during the TCS-08 field project. The hourly estimates of intensity (maximum sustained 1-min surface winds) were used to monitor the typhoon's rapidly changing behavior during missions. The current intensity T number (CI#, blue line) is related to actual intensity through the Dvorak conversion and is used as the final intensity estimate. The adjusted T number (AdjT#, green line) is an intermediate parameter used in the CI# process [see Olander and Velden (2007) for further details on the ADT].

Table 1. Intercomparison of approximate microwave image and sounder spatial footprint sizes (km) and swath widths for the current constellation of sensors (actual values are oval shaped and have been generalized here). Note the disparity between the research and development (R&D) sensors (TMI, AMSR-E, and WindSat) and the operational sensor suite (SSM/I and SSMIS).

Channel sensor	6–7 GHz	10–11 GHz	18–19 GHz	22–24 GHz	36–37 GHz	85–91 GHz	150 GHz	Swath (km)
SSM/I			56	50	33	12		1,400
SSMIS			55	55	35	12	13	1,700
TMI		50	24	20	12	5		800
AMSR-E	50	50	25	25	15	5		1,800
WindSat	55	40	20	13	11			1,025
AMSU-B						16*	16*	2,300

* AMSU-B is a sounder with inherently poorer resolution and the values noted are for nadir only; values near the edge of scan can reach 26 × 50 km^2.

imagery, contain only small ice crystals, so that the 85–91-GHz channels can readily sense through these upper clouds to depict areas of intense deep convection with a higher content of frozen precipitation.

The operational Defense Meteorological Satellite Program (DMSP) LEO spacecraft carry the Special Sensor Microwave Imager (SSM/I) and the more recent Special Sensor Microwave Imager Sounder (SSMIS). As noted in Table 1, both sensors contain an ice-scattering channel (85 and 91 GHz, respectively). Modest temporal TC sampling was possible during T-PARC/TCS-08 because of the availability of three SSMI sensors (on board the F-13, F-14, and F-15 spacecraft; 1,400-km swath) and two SSMIS sensors (F-16 and F-17; 1,700-km swath). Table 1 shows the 85–91-GHz spatial fields of view are ~12 km and except for very small eyewalls, they can adequately sample most TC features.

Supplementing the operational microwave imagers is a suite of research sensors. The Navy's WindSat polarimetric radiometer on the Coriolis spacecraft is the first mission to test surface wind vector retrievals via a passive sensor (Gaiser et al. 2004). Near-real-time WindSat wind vectors and high-resolution 37-GHz imagery (which can highlight low-level cloud liquid water) assisted the field program in monitoring rainband and eyewall structures (Hawkins et al. 2006; Turk et al. 2006),

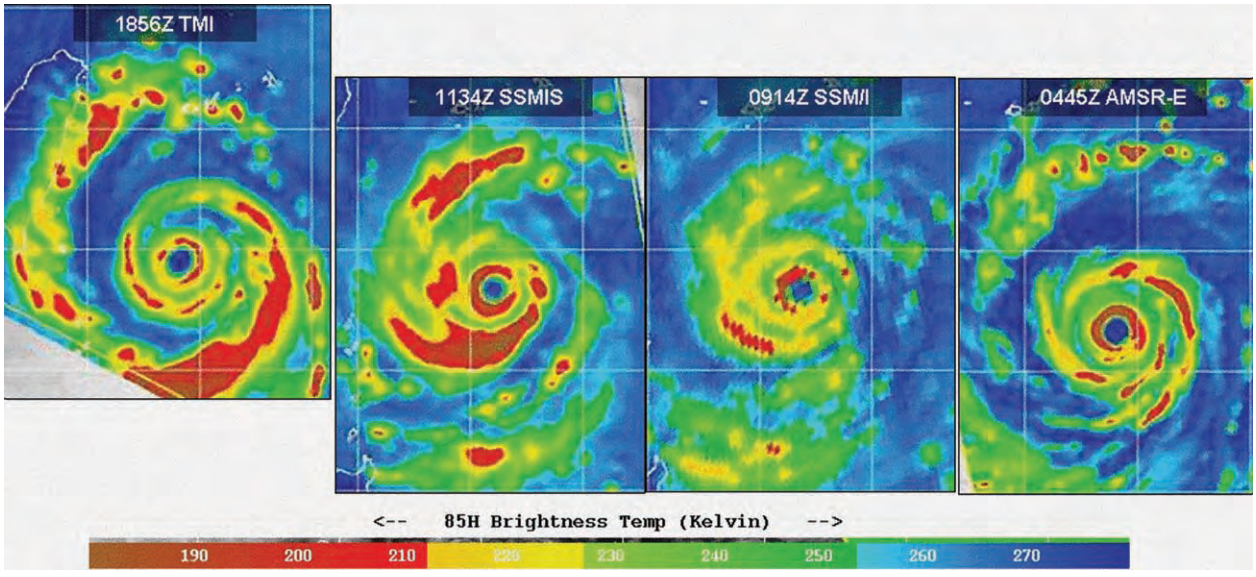

Fig. 4. Example of ice-scattering channels from AMSR-E, SSM/I, SSMIS, and TMI for (right to left) 0445, 0914, 1134, and 1856 UTC, respectively, during Typhoon Jangmi on 27 Sep 2008. All four images have the same scale and projection, with 2° latitude and longitude lines in white.

while the radiometer also produced sea surface temperatures (SSTs). The National Aeronautics and Space Administration's (NASA) Tropical Rainfall Measuring Mission (TRMM) Microwave Imager (TMI) has an approximate 6-km spatial field-of-view resolution at 85 GHz across its 800-km swath (Lee et al. 2002), SSTs, and potentially multiple views per day. TMI data are complemented by the Advanced Microwave Scanning Radiometer for Earth Observing System (EOS; AMSR-E) launched on board the NASA EOS *Aqua* platform in May 2002 that combines a much larger 1800-km swath with TMI-like spatial resolution (Table 1), making the sensor a major boon to TC monitoring because of its resolution, swath attributes, and SST attributes.

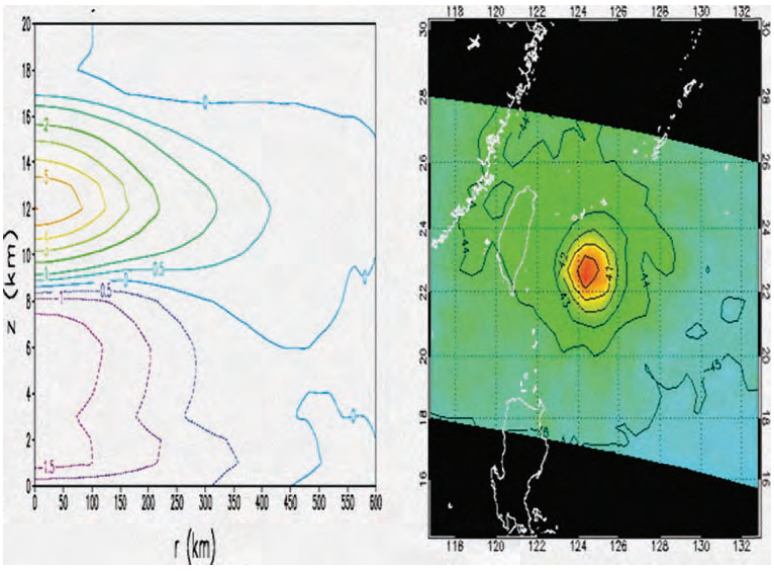

Fig. 5. Representation of (left) AMSU-A retrieved vertical temperature anomaly from CIRA and (right) the horizontal raw T_B anomaly for channel 8 (~150 hPa) from CIMSS for Typhoon Sinlaku (JTWC 15W) on 11 Sep 2008.

Figure 4 displays four 85–91-GHz horizontal polarization (H-Pol) examples from the AMSR-E, SSM/I, SSMIS, and TMI (right to left with time as Super Typhoon Jangmi approaches Taiwan). The microwave imager views enabled the T-PARC/TCS-08 operations center to monitor concentric eyewall evolution during a coincident WC-130J aircraft mission. Figure 4 highlights a double-eyewall configuration with a stable inner eyewall, while the outer western band intensifies, likely partially attributable to enhanced low-level convergence that is topographically induced.

Microwave sounder datasets. Microwave sounder data from the National Oceanic and Atmospheric Administration (NOAA) series of operational polar orbiters can serve multiple TC monitoring functions: i) to create imagery using sounder channels that are unique in frequency compared to microwave imager channels, ii) to utilize temperature sounding capabilities (i.e., a 55-GHz band to extract TC intensity estimates, and iii) to produce rainfall estimates from multichannel retrievals. The Advanced Microwave Sounding Unit (AMSU), a NOAA LEO mainstay, has channels sensitive to both temperature (AMSU-A1/A2) and moisture (AMSU-B). The AMSU-B sensor has an 89-GHz channel; however, the nominal resolution is ~16 (nadir) and 50 km at the edge of the swath. This cross-track scanner (sweeps back and forth from one side to another) can resolve TC features to varying degrees depending on where in the viewing swath the TC is located, but not with the detail and precision of the aforementioned imagers; however, it does provide enhanced temporal sampling.

The AMSU-retrieved temperature data can be used to observe a TC's warm inner core and, via hydrostatic approximations, infer storm intensity. Recent attempts at quantifying this relationship have led to two intensity estimation algorithms that have become competitive with the longstanding and operational IR-based Dvorak technique. These techniques rely on the magnitude of the AMSU-A observed warm core (Fig. 5) and are further described in DeMuth et al. (2006) and Herndon et al. (2004). Since routine western North Pacific aircraft TC reconnaissance flights ceased in summer 1987, the AMSU methods have not been directly validated in this basin. Therefore, the T-PARC/TCS-08 field experiment provided an excellent opportunity to calibrate and verify these algorithms in the western North Pacific. In addition, this effort benefited the validation of an experimental satellite consensus (SATCON) method that uses a weighted average of ADT and the two AMSU estimates and has proven superior when using Atlantic reconnaissance validation data (Herndon et al. 2010). SATCON was operating in real time during the field campaign, and a post-experiment validation analysis using a limited set of reconnaissance observations as ground truth found that SATCON was superior to all other satellite-based methods, including the operational Dvorak estimates (Herndon et al. 2010).

Quick Scatterometer (QuikSCAT) and Advanced Scatterometer (ASCAT). Microwave scatterometers can infer near-surface wind vectors that can help monitor low-level circulation centers, TC genesis, the radius of gale winds, and storm intensity. Scatterometers are active microwave radars that transmit pulses, measure the backscattered energy emitted by the ocean, and gather the response from multiple looks or scanning geometry. The backscatter response is largely a function of surface roughness, which is driven principally by small centimeter-scale waves that are mainly in equilibrium with the local wind stress and depend on both the wind speed (scalar) and wind direction (why multiple looks are required). The NASA SeaWinds scatterometer on the QuikSCAT satellite performed flawlessly for more than a decade (July 1999) but failed in November 2009 (after the T-PARC/TCS-08 project). QuikSCAT operated at 13.4 GHz and had a 1,800-km swath, making approximately 400,000 measurements and covering 90% of Earth's surface daily.

During T-PARC/TCS-08, the NRL acquired 25-km QuikSCAT wind vectors from the Fleet Numerical Meteorology and Oceanography Center (FNMOC) and 12.5-km wind vectors from NOAA with a data latency (time from satellite view to product dissemination) of 1–3 h and created the following products: i) wind vectors overlain on VIS/IR imagery, and both 85- and 37-GHz microwave brightness temperature imagery (when coincident passes occur within ±3 h; and ii) wind vector ambiguities (up to four solutions) overlain on the same suite of background imagery while denoting which observations are "rain flagged." Figure 6 illustrates QuikSCAT wind vectors overlain on *MTSAT IR* imagery on 26 September 2008 for Super Typhoon Jangmi (JTWC 19W). The color-coded winds assist the satellite analyst in deriving gale wind radii. Figure 6 also depicts the relative wind minimum between the eyewall and the main northern rainband. QuikSCAT's Ku-band frequency is susceptible to rain contamination; however, when winds are typhoon force or stronger, the rain impact causes fewer interpretation problems than at 20–30 kt. In addition, 2.5-km experimental wind vectors were acquired from Brigham Young University.

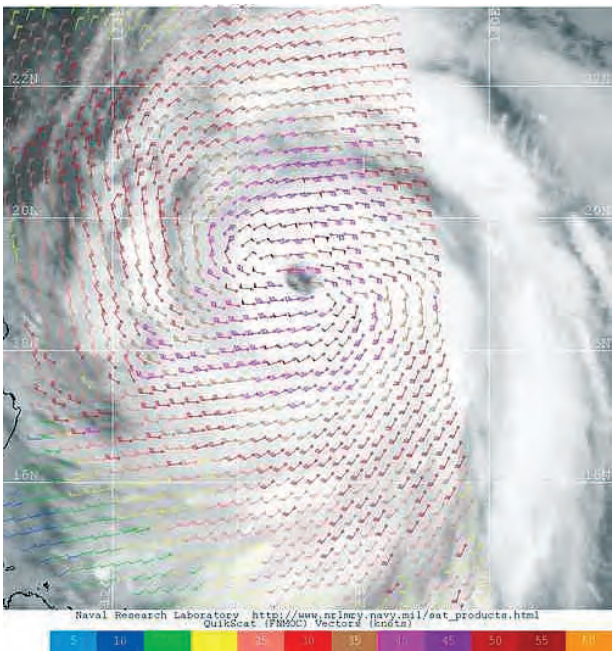

Fig. 6. Example of 25-km-resolution QuikSCAT ocean surface wind vectors overlain on MTSAT visible imagery for Tropical Storm Jangmi at 2152 UTC 26 Sep 2008. The wind vectors are color coded by wind speed (kt) to assist the analyst in quickly noting high winds. Wind vectors flagged for possible rain contamination are denoted with a circle at the tail of the wind barb or stick.

The European Space Agency's Meteorological Operation (MetOp) ASCAT (July 2006 launch) sensor has an 1,100-km swath with a unique configuration: twin 550-km swaths to each side of nadir, separated by a 672-km "hole" or area of no wind retrievals. This C band (5.255 GHz) radar is less susceptible to rain contamination, but it has coarser spatial resolution because of its frequency selection. Routine 50-km spatial-resolution oceanic surface wind vectors were available during T-PARC/TCS-08 and experimental 25-km-resolution winds were also available. The near-real-time ASCAT digital dataset was provided via collaborative agreements with the European Organisation for the Exploitation of Meteorological Satellites (EUMETSAT) and NOAA.

CloudSat cloud radar. NASA's *CloudSat* Earth system pathfinder mission utilizes a millimeter-wavelength cloud radar to advance our understanding of cloud abundance, distribution, structure, and radiative properties (Stephens et al. 2002). *CloudSat*'s radar is 1,000 times more sensitive than existing weather radars with a nadir-only view (2.5×1.4-km^2 spot) and 500-m vertical resolution (interpolated to 240 m). *CloudSat* maps the cloud top/base and areal extent, light and moderate rain, the freezing level, convective tower locations, and rain-free zones during its TC overpasses. During T-PARC/TCS-08, near-real-time (4–6-h data latency) digital *CloudSat* data were made available by the Cooperative Institute for Research in the Atmosphere (CIRA) and provided crucial vertical cloud structure information along its nadir track (no swath).

NRL created vertical cross sections of radar reflectivity with graphics that merged the *CloudSat* data with coincident MTSAT, Moderate Resolution Imaging Spectroradiometer (MODIS) VIS/IR imagery, and AMSR-E 89-GHz brightness temperatures (Mitrescu et al. 2008). In Fig. 7 AMSR-E effectively maps the two-dimensional rainband and eyewall structure, while *CloudSat* maps a narrow vertical profile and highlights the following features: i) the "rain free" microwave eye is covered with ice clouds aloft, ii) the eyewalls are tilted outward with height, iii) the southern eyewall has an embedded vigorous convective tower that extends well above 15 km, iv) a "moatlike" region just north of the eyewall has rain depicted at lower levels in the *CloudSat* data, and v) strong convective towers are evident in multiple locations along the transect and agree with lower AMSR-E brightness temperature caused by ice scattering. This dataset nicely complements the 3D wind, rain, and cloud microphysical information derived from the NRL P-3-based Electra Doppler Radar (ELDORA). In addition, NASA TRMM precipitation radar (PR) rain rates were available in near–real time via the NRL TC Web page under the "rain" link, while full vertical slice digital data were available from the following Web site (click on QuickTime animation at the bottom of the Web page): http://trmm.gsfc.nasa.gov/publications_dir/multi_resource_tropical.html.

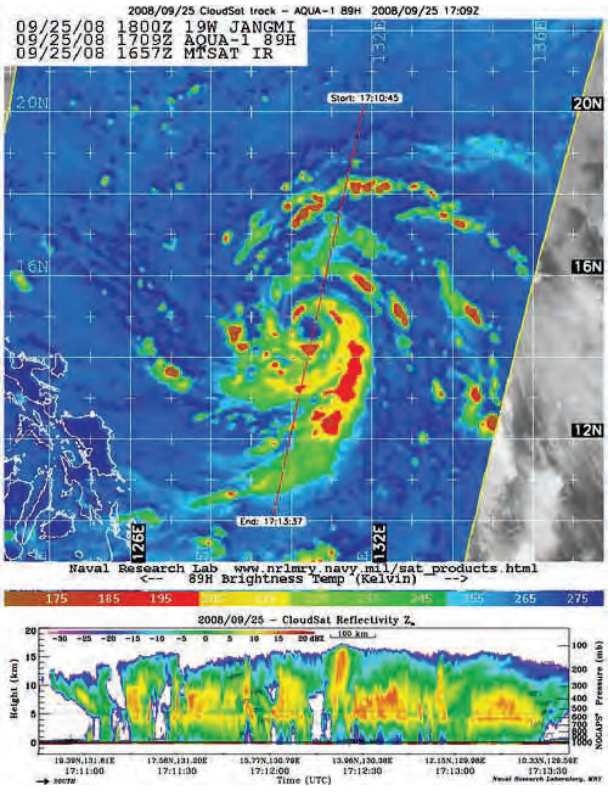

Fig. 7. (top) The CloudSat ground track is overlain on a coincident AMSR-E 89-GHz T_B image. The radar overpass travels from north to south and intersects the "relatively" rain-free eye while highlighting an intense convective burst in the southern eyewall. (bottom) A *CloudSat* cloud radar reflectivity vertical cross section (altitude scale 0–20 km) for a transect through Super Typhoon Jangmi at 1709 UTC 25 Sep 2008. (data courtesy of the CSU CloudSat Data Processing Center).

Altimeter SSH and ocean heat content. Spaceborne altimeters have been used for several decades to accurately measure global sea level heights. The altimeter measures the range between the satellite and the ocean surface, and knowledge of the satellite height above the reference ellipsoid (a mathematically defined surface that approximates the geoid or the equipotential surface, which would coincide exactly with the mean ocean surface of Earth if the oceans were in equilibrium, at rest, and extended through the continents) provides a value for sea level height. Accurate knowledge of Earth's geoid then provides the ability to compute the sea surface height (SSH) values needed to monitor mesoscale oceanic currents and eddies that can impact TC intensity. Altimeters frequently use exact repeat missions (constrain orbit to within ±1 km along a preset track) to mitigate geoid errors and view sea level changes or deviations relative to a mean reference surface.

Shay et al. (2000) and others have shown that these SSH measurements can be used to estimate oceanic heat content (OHC) variations that are linked to TC intensity change and rapid intensification and weakening. Sea surface topography from multiple altimeters takes advantage of their multiple spatial and temporal sampling scales. When cast within a two-layer ocean model, the depth of the 26°C isotherm can be estimated from these objectively analyzed and mapped SSH anomaly fields. Using monthly, seasonal, or annual climatologies, the integrated thermal structure or OHC can be estimated from that depth to the surface where the SST is used as the surface boundary condition. This approach provides the locations of warm and cold features in front of the projected track of tropical cyclones, as discussed in Shay and Uhlhorn (2008). The uncertainties in these estimations are within 10%–15% of in situ measurements from buoys, floats, and expendables.

Near-real-time SSH maps were available during T-PARC/TCS-08 to monitor mesoscale ocean front and eddy activity, provided courtesy of the NRL–Stennis Space Center (Ko et al. 2008). Shown in

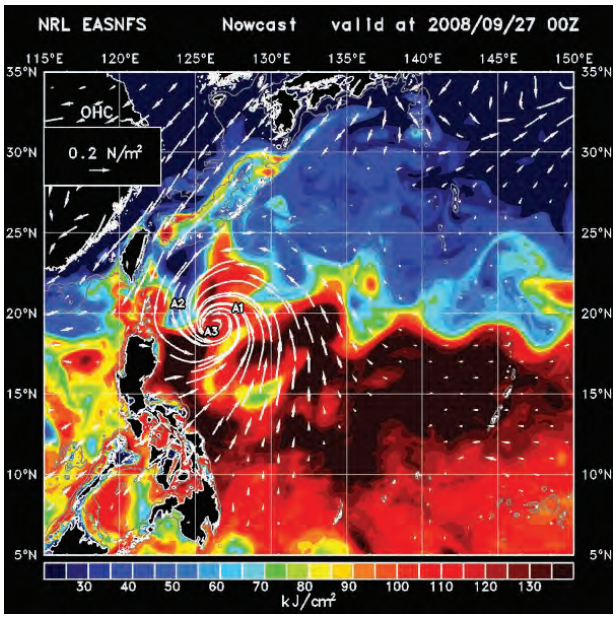

Fig. 8. OHC map on 27 Sep 2008 for a western North Pacific domain during Typhoon Jangmi provided by NRL-SSC. The dataset assimilates multiple altimeter SSH measurements into an ocean model nowcast product. The navy's Operational Global Atmospheric Prediction System (NOGAPS) surface wind stress vectors are overlain in white (see reference scale) (courtesy: Ko).

Fig. 8 is an example of Super Typhoon Jangmi on 27 September 2008 (high OHC values—orange/brown, low values—blue). T-PARC/TCS-08 utilized the near-real-time OHC product in selecting locations to place aircraft-deployed airborne expendable bathythermograph (AXBT, probes that measure temperature from the surface down to 1,000 m) and floats/buoys with multiple sensors at depth to map mesoscale ocean features and to capture critical regions of air–sea interaction during TC conditions.

Tailored Web pages for satellite product portals. To provide efficient real-time portals for viewing the extensive satellite data and products during T-PARC/TCS-08 mission planning, nowcasting, and forecasting, tailored Web sites were developed by NRL and CIMSS. These sites were spinoffs of their real-time TC Web pages that are used globally to monitor storms. These portals were also used as postevent browsers to facilitate swift perusal of all the available comprehensive satellite products and datasets. The two Web sites specialize in different areas of satellite data and product displays; therefore, they are quite complementary, especially when used together to support a field campaign.

NRL at Monterey (NRL-MRY). Since 1997, NRL-MRY has been providing near-real-time, storm-centered satellite imagery products via the Web. The portal utilizes TC and invest locations retrieved from the Automated Tropical Cyclone Forecast (ATCF) system (Sampson and Schrader 2000) to "storm center" all satellite products. Users are presented with a graphical user interface that permits them to select the storm of interest and view a suite of passive microwave and VIS/IR products that are all collocated for the storm of interest (see Fig. 9). The "pass_mosaic" function displays the most recent 24 h of microwave images (85–91-GHz default), and the user can click on any of the thumbnail versions to view a larger display. Background processing algorithms automatically update the Web page with new products as they become available asynchronously.

The Web site's main focus is the suite of microwave imagery [ice-scattering channels, 37 GHz, polarization-corrected temperature (PCT), which isolates the effect of the signal attenuation from hydrometeors and removes the effect of surface temperatures] and "color" mosaic and derived products [rain rate, surface wind speed, and total precipitable water (TPW)]. The site also includes DMSP nighttime visible data, which can assist in nocturnal center fixing. Ocean surface wind vectors from all available scatterometer sensors can be displayed in overlay form to permit the user to extract gale-force wind radii estimates and storm size (for real-time examples, see www.nrlmry.navy.mil/TC.html).

A derivative of the NRL-MRY TC page was developed for the T-PARC/TCS-08 experiment. More than 60 individual invest areas (some of which became targeted TCs) were processed during the T-PARC/TCS-08 project. The NPS operations center decided which cloud systems were to be monitored by electronically sending a short message to NRL-MRY. The latitude/longitude position and invest number would automatically "open up" a new domain or invest region within which a suite of satellite products were created and posted to the Web. The invest locations were then routinely updated and the domains eventually deactivated when project interest terminated. (The NRL-MRY Web page for T-PARC/TCS-08 can be found at www.nrlmry.navy.mil/tcs-bin/tcs_home2.cgi.)

The Web site also includes Google Earth capabilities (Turk et al. 2010) that were used for the first time to support a field project during TCS-08. The use of satellite product keyhole markup language (KML) files helped to visualize multiple datasets: planned flight tracks and expendable probe locations (dropsondes, AXBTs, and drifting buoys), real-time flight tracks

for in-flight track adjustments and multiplane coordination, and numerical weather prediction model field overlays. Figure 10 illustrates real-time aircraft track overlays using microwave imagery that was crucial in safely guiding the NRL P-3 into the relatively convection-free sector of Tropical Storm Jangmi. The NRL P-3 and its highly capable ELDORA were not designed to transit through TC eyewalls, thus the real-time satellite KML files greatly aided the scientific mission while maintaining plane/crew safety. The Google Earth capability was also utilized in the Impact of Typhoons on the Ocean in the Pacific (ITOP), the Pre-Depression Investigation of Cloud-systems in the Tropics (PREDICT), the Intensity Forecasting Experiment (IFEX), and the Genesis and Rapid Intensification Processes (GRIP) TC field projects in both the Atlantic and western Pacific during the summer of 2010.

University of Wisconsin—Madison's CIMSS. The CIMSS tropical cyclones Web site was introduced in 1993 and was the first known public site devoted to TC monitoring. The site has recently been updated and includes both regional product displays and an interactive storm window that users can manipulate. Active storms and invests are displayed as icons on a global map. Users can click on these icons to activate the interactive window for a system of interest. The window product suite includes a wide array of real-time TC-relevant data and analyses that can be overlain on various options of satellite imagery and/or derived analyses. Users can also view larger-scale imagery, analyses, and products via a Web interface that covers each TC basin. A suite of imagery, diagnostic products, and overlays permits users to interrogate the environmental conditions encompassing each TC

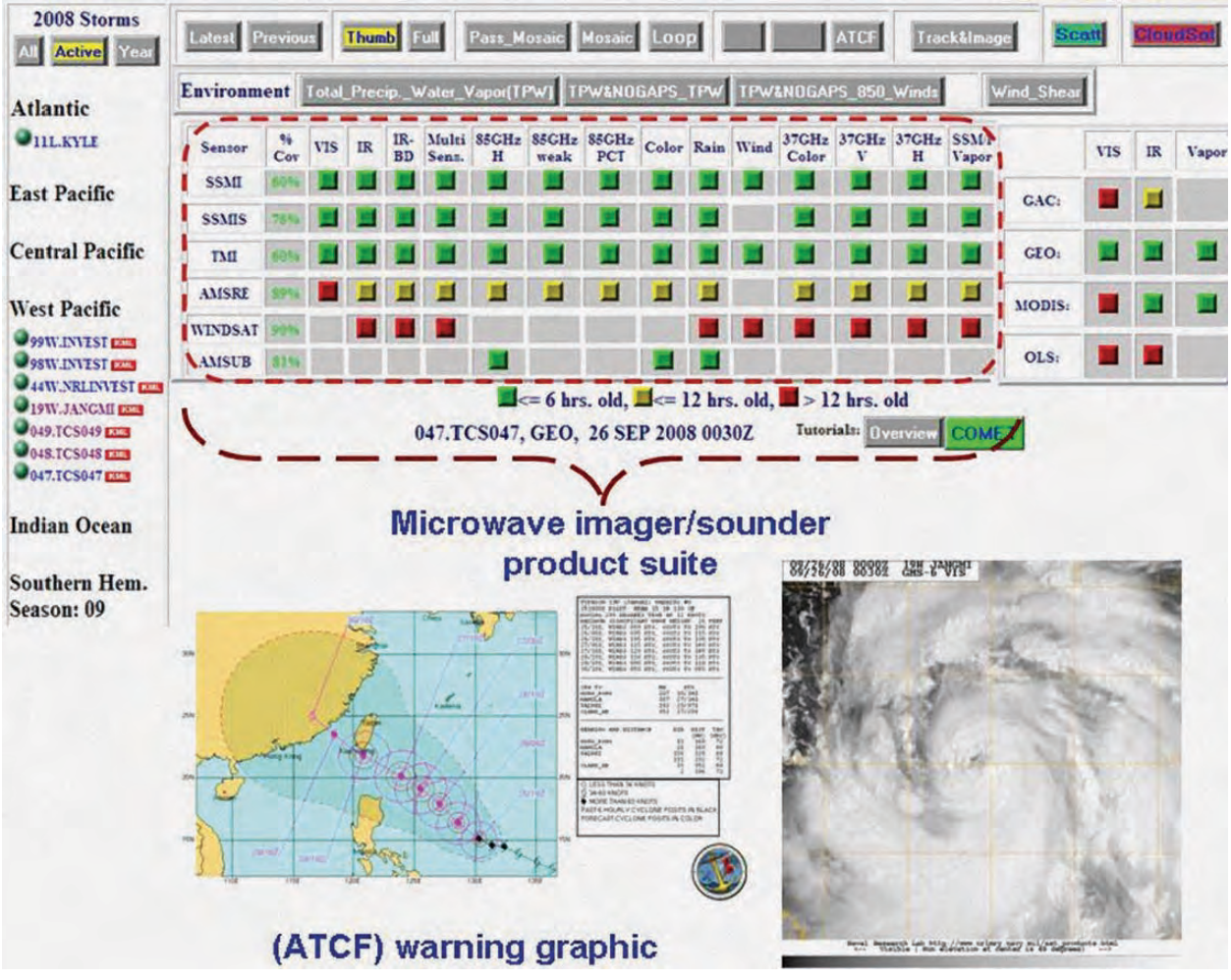

Fig. 9. Sample NRL-MRY T-PARC/TCS-08 satellite Web page on 26 Sep 2008 during Super Typhoon Jangmi's journey through the field project domain. (left) A list of active named storms and invests initiated by JTWC and the TCS-08 invests, (top center) the suite of passive microwave products, (right) the VIS/IR imagery datasets, (bottom left) the ATCF track graphics, and (bottom right) the latest VIS/IR image products. The microwave and VIS/IR buttons are color coded to denote data latency.

(for real-time examples, see the CIMSS TC Web page at http://tropic.ssec.wisc.edu).

A derivative of the CIMSS TC page was developed for the T-PARC/TCS-08 experiment, with a focus on the western North Pacific domain. The interactive window displays were used daily in the NPS operations center for projecting current conditions over potential or ongoing invests. Special products such as the real-time hourly high-resolution MTSAT cloud-drift winds and derived diagnostics produced at CIMSS were also made available via this interface (Fig. 11) [a clone of this site, now active and supporting the Joint Typhoon Warning Center (JTWC), can be found at http://cimss.ssec.wisc.edu/tropic2/tparc/tparc.php].

OTHER SITES. While not associated with the T-PARC/TCS-08 experiment, other valuable Web sites provide access to real-time satellite data and products that have been used to support meteorological field programs. A good example is the NASA Marshall Space Flight Center (MSFC) Real Time Mission Monitor (RTMM), which includes Google Earth projections. The RTMM is a situational awareness tool that integrates satellite, airborne, and surface datasets; weather information; model and forecast outputs; aircraft waypoint planning; and real-time location data for airborne field experiment management (http://rtmm.nsstc.nasa.gov/index.html).

Another recent NASA site derived for TC investigations by the Jet Propulsion Laboratory (JPL) is referred to as the Tropical Cyclone Information System (TCIS) and includes coincident numerical model fields and tools to display/analyze them together (http://tropicalcyclone.jpl.nasa.gov). This site can be tailored further for the support and postanalysis of specific missions (e.g., see http://grip.jpl.nasa.gov).

POST–FIELD EXPERIMENT ANALYSIS, DATA BROWSING, AND ARCHIVES. In addition to the value of satellite observations in real-time monitoring, post–field experiment analyses can benefit from the integration of quantities in the form of geophysical parameters or fields derived from the digital data. The many satellite-derived products discussed above can be important "gap fillers" in four-dimensional analyses of field experiment observations, since those observations are often limited in spatial and temporal coverage. For example, CIMSS postprocessed the *MTSAT-2* rapid-scan atmospheric motion vectors for all available periods during T-PARC/TCS-08. The very high spatial and temporal resolution of these datasets can capture TC flow details (see Fig. 2) and complement the aircraft flight-level and dropsonde wind information in high-resolution 4D data assimilation and numerical model forecast studies. Many of the other satellite-derived products (e.g., Table 2) could contribute in a similar manner.

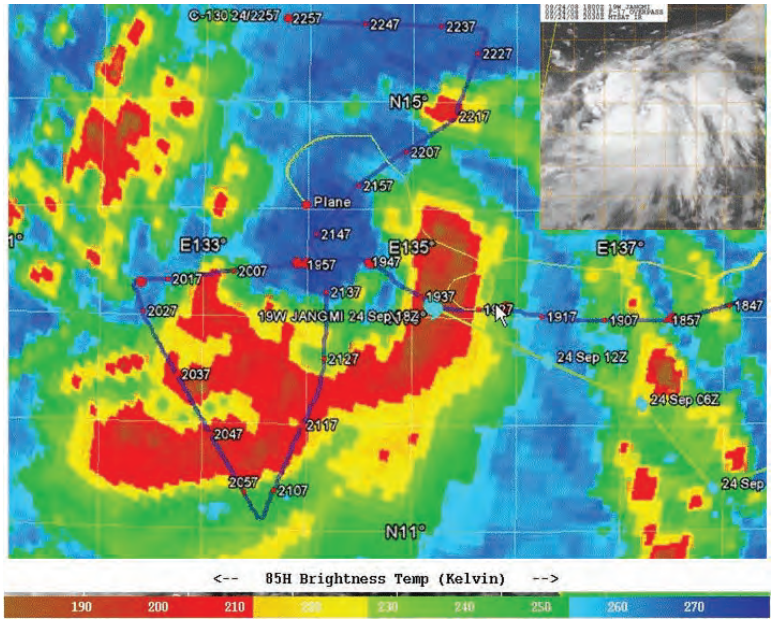

FIG. 10. F-16 SSMIS 91-GHz H-pol T_B image at 2031 UTC 24 Sep 2008 during TC Jangmi. The red, yellow, and green areas outline major rainbands and the developing eyewall, while the blue areas represent nonconvective zones. The blue line is the WC-130J aircraft track marked every 10 min, while the thin yellow line denotes the NRL P-3 aircraft track while it traverses safely into the north sector free of potentially hazardous convective cells. The corresponding IR image is located in the top-right corner.

Most of the collected T-PARC/TCS-08 data reside at the NCAR Earth Observing Laboratory, the field program's official data management and archive facility. For the satellite data, NRL-MRY provided Joint Photographic Experts Group (JPEG) browse products, KML files, and digital data; examples are listed in Table 2. The CIMSS images and products were provided as graphic interchange format (GIF)/tagged image file format (TIFF) images, while MTSAT AMVs were provided as American Standard Code for Information Interchange (ASCII)-formatted text files. Users can order archived satellite data directly through the EOL archive or can

follow active links that direct users to the appropriate archive center. The T-PARC/TCS-08 field catalog, which contains reports and products produced during the campaign, is online (http://catalog.eol.ucar.edu/tparc), as is the EOL data archive, which contains the raw data (Table 3) (www.eol.ucar.edu/projects/t-parc/).

SUMMARY. Satellite-based remote sensing played a key role in supporting the western North Pacific operations of the T-PARC/TCS-08 field program in 2008, as well as in supplementing postmission analyses of observed typhoon events and contributing to the project's scientific goals. Aircraft mission planning, flight direction, nowcasting, and forecasting for the project were all reliant on a suite of multispectral satellite imagery and products brought to the field by dedicated Web-based sites. These sites allowed the integration of diverse datastreams for fusion into derived graphics and illustrations for investigator analysis and real-time decision making. The T-PARC/TCS-08 example discussed in this paper is just one of many weather-related projects that are making increasing use of remotely sensed satellite data and products for field operations support. In 2010, for instance, a follow-up experiment to TCS-08 was conducted (TCS-10) and included the Impact of Typhoons on the Ocean in the Pacific (ITOP) field program. Satellite data were a critical observational component for investigating both the atmospheric and oceanographic components. Another great example was the recently completed multiagency TC field experiment in the Atlantic Ocean in 2010, composed of PREDICT, sponsored by the National Science Foundation (NSF), GRIP, sponsored by NASA, and IFEX, sponsored by NOAA. All of the Web sites listed above provided satellite data and product support to these major exercises. In addition, newly developed satellite-derived tools were unveiled, including animated total precipitable water and detection of overshooting tops. Both products were used extensively to help direct aircraft and will be invaluable postanalysis datasets.

While the above examples are primarily TC-oriented projects, the opportunities for optimized

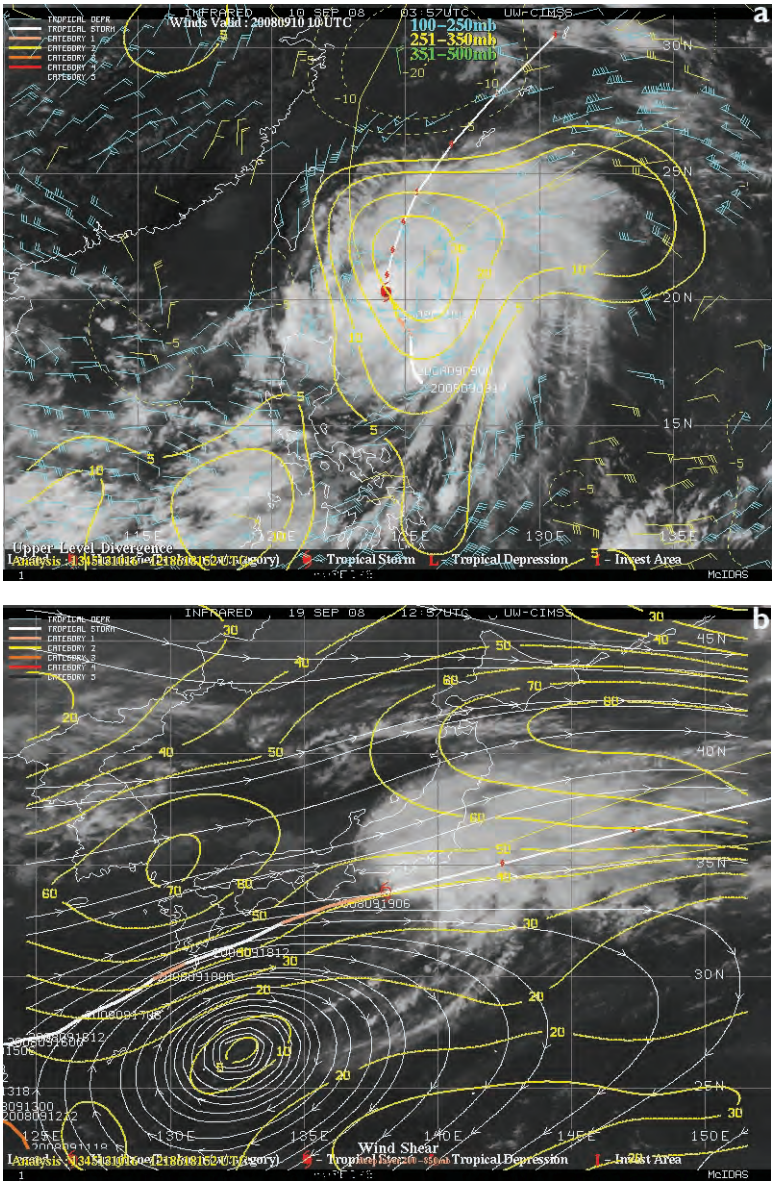

Fig. 11. Examples of the CIMSS interactive Web page display available in the T-PARC/TCS-08 operations center during TC Sinlaku: (a) MTSAT IR image overlain with AMVs and derived upper-level divergence (yellow contours) and (b) MTSAT IR image overlain with the storm track of Sinlaku and with a deep-layer shear analysis (streamlines in white; isotachs knots in yellow) derived using the high-resolution MTSAT AMVs valid 1300 UTC 19 Sep 2008. The operations center analysts and forecasters used this capability on a daily basis during the field program to display a variety of satellite products in tandem with conventional observations to assess current conditions and for mission planning.

Table 2. Example satellite EOL catalog browse products during T-PARC/TCS-08. AVHRR = Advanced Very High Resolution Radiometer; DMSP OLS = Operational Line-Scanning System; GAC = global area coverage.

Instrument	Channel/product	Spatial resolution	Temporal resolution	File format
MTSAT-1R	1	1 km	30 min	JPEG
MTSAT-1R	3, 4	4 km	30 min	JPEG
MTSAT-1R	Cloud-drift winds	Low level/Upper level	6 hourly	TIFF
MODIS	1,2	250 m	~2 per day	JPEG
MODIS	True color mosaic	500 m	~2 per day	JPEG
MODIS	Infrared	1 km	~2 per day	JPEG
AVHRR	VIS/IR	4 km GAC	~2 per day per satellite	JPEG
DMSP OLS	VIS/IR nighttime VIS	2.8-km smooth	~2 per day per satellite	JPEG
QuikSCAT	Surface wind vectors	12, 25 km	0–2 per day	JPEG and ASCII
ASCAT and WindSat	Surface wind vectors	25, 50 km	0–2 per day	JPEG and ASCII
AVHRR	SST composite	6 km	Daily	JPEG
Microwave sensors (all)	37, 85–91 GHz, PCT, color	6–35 km	5–12 per day per system	JPEG
Microwave sensors (all)	Wind speeds, rain rate, TPW	6–35 km	5–12 per day per system	JPEG
CloudSat	Radar cross sections	500-m vertical nadir only	Infrequent	JPEG
Polar-orbiting satellites	Daily overpass times	—	—	Table

Table 3. Example satellite digital data and derived products archived at NCAR EOL for the T-PARC/TCS-08 period (Aug–Oct 2008). NetCDF = network Common Data Form; L1b = level 1b; AFWA = Air Force Weather Agency.

Instrument	Channel/product	Archived resolution (km)	Units	File format	Comments, real-time source
MTSAT-1R	1	1, 4	Albedo	netCDF	Via UW-CIMSS; raw data are not saved at EOL, only calibrated units
MTSAT-1R	2, 3, 4, 5	4	T (°C)	netCDF	
MTSAT-1R	AMVs		m s^{-1}	ASCII	Via UW-CIMSS
MTSAT-2R	1	1, 4	Albedo	netCDF	Via UW-CIMSS; raw data are not saved at EOL, only calibrated units
MTSAT-2R	2, 3, 4, 5	4	T (°C)	netCDF	
MTSAT-2R	AMVs		m s^{-1}	ASCII	Via UW-CIMSS
AVHRR	1–5	4	Raw	L1b	Via NOAA class system
DMSP OLS	VIS, IR	2.8	Raw	netCDF	Via FNMOC/AFWA
MODIS	VIS, IR	1	Albedo/T °C	netCDF	Via NOAA NRTPE
Microwave all sensors	6–91-GHz T_B	6–35	T (K)	netCDF	Via FNMOC/AFWA
Microwave all sensors	Wind speed, rain rate, TPW	25	m s^{-1}, mm h^{-1}, mm	ASCII	Via FNMOC/AFWA
QuikSCAT, ASCAT, WindSat	Surface wind vectors	12, 25, 50	m s^{-1}, direction (°)	ASCII	Via FNMOC and NOAA

satellite datasets and tailored products can span the full range of meteorological applications. In scientific studies, satellite data are often thought of only in terms of conventional imagery. However, as this paper illustrates, there is a variety of both operational and research datasets and derived products that can depict current atmospheric conditions and enhance targeted in situ datasets in research field programs. The list continues to grow as new sensors and instruments are deployed, calibrated/validated, and brought online. Assimilation of these datasets into high-resolution analyses for use in process studies should decrease the chances of deficient analyses, permit the evaluation of innovative new hypotheses, and increase confidence and fidelity in study results.

ACKNOWLEDGMENTS. We would like to acknowledge NOAA for making available the QuikSCAT, AVHRR LAC/GAC, and AMSU digital data from the NOAA LEO satellites, as well as redistributing the EUMETSAT ASCAT and ERS-2 data in near–real time; NASA for providing TRMM data via the TRMM Science Data and Information System (TSDIS) and AMSR-E via the Near Real Time Processing Effort (NRTPE); AFWA/FNMOC for supplying and processing the SSM/I, SSMIS, and OLS data; FNMOC for facilitating access to the Windsat data. *CloudSat* cloud radar data are available via collaboration with Colorado State University's (CSU) CloudSat Data Processing Center. The MTSAT imagery used during T-PARC/TCS-08 was kindly provided by the Japan Meteorological Agency. Dave Stettner and Derrick Herndon of UW-CIMSS were instrumental in providing data and product flow to the T-PARC/TCS-08 campaign. The NRL TC Web team (Kim Richardson, Tom Lee, Charles Sampson, Mindy Surratt, John Kent, Richard Bankert, Jeremy Solbrig, Steve Miller, and Arunas Kuciauskas) all contributed to the NRL TCS-08 Web products. Pat Harr and Peter Black were instrumental in incorporating the suite of satellite products into daily operations. The authors' T-PARC/TCS-08 satellite support efforts were sponsored by the Office of Naval Research's (ONR) Marine Meteorology Program and leverage other programs sponsored by PEO C4I&SPACE PMW-120 and the NOAA Joint Polar Satellite System (JPSS).

REFERENCES

Demuth, J. L., M. DeMaria, and J. A. Knaff, 2006: Improvement of Advanced Microwave Sounding Unit tropical cyclone intensity and size estimation algorithms. *J. Appl. Meteor. Climatol.,* **45,** 1573–1581.

Gaiser, P. W., and Coauthors, 2004: The WindSat spaceborne polarimetric microwave radiometer: Sensor description and early orbit performance. *IEEE Trans. Geosci. Remote Sens.,* **42,** 2347–2361.

Hawkins, J., M. Helveston, T. F. Lee, F. J. Turk, K. Richardson, C. Sampson, J. Kent, and R. Wade, 2006: Tropical cyclone multiple eyewall configurations. Preprints, *27th Conf. on Hurricanes and Tropical Meteorology,* Monterey, CA, Amer. Meteor. Soc., 6B.1. [Available online at http://ams.confex.com/ams/27Hurricanes/techprogram/paper_108864.htm.]

——, C. Velden, and T. Nakazawa, 2009: Satellite digital data and products for tropical cyclone studies. Preprints, *Second Int. Workshop on Tropical Cyclone Landfalling Processes (IWTCLP-II),* Shanghai, China, WMO, 131–142.

Herndon, D. C., C. S. Velden, K. Brueske, R. Wacker, and B. Kabat, 2004: Upgrades to the UW-CIMSS AMSU-based tropical cyclone intensity algorithm. Preprints, *26th Conf. on Hurricanes and Tropical Meteorology,* Miami, FL, Amer. Meteor. Soc., 4D.1. [Available online at http://ams.confex.com/ams/26HURR/techprogram/paper_75933.htm.]

——, ——, J. Hawkins, T. Olander, and A. Wimmers, 2010: The CIMSS Satellite Consensus (SATCON) tropical cyclone intensity algorithm. *29th Conf. on Hurricanes and Tropical Meteorology,* Tucson, AZ, Amer. Meteor. Soc., 4D.4.[Available online at http://ams.confex.com/ams/29Hurricanes/techprogram/paper_167959.htm.]

Ko, D. S., P. J. Martin, C. D. Rowley, and R. H. Preller, 2008: A real-time coastal ocean prediction experiment for MREA04. *J. Mar. Syst.,* **69,** 17–28.

Lee, T. F., F. J. Turk, J. D. Hawkins, and K. A. Richardson, 2002: Interpretation of TRMM TMI images of tropical cyclones. *Earth Interact.,* **6.** [Available online at http://EarthInteractions.org.]

Mitrescu, C., S. Miller, J. Hawkins, T. L'Ecuyer, J. Turk, P. Partain, and G. Stephens, 2008: Near-real-time applications of *CloudSat* data. *J. Appl. Meteor. Climatol.,* **47,** 1982–1994.

Olander, T. L., and C. S. Velden, 2007: The advanced Dvorak technique: Continued development of an objective scheme to estimate tropical cyclone intensity using geostationary infrared satellite imagery. *Wea. Forecasting,* **22,** 287–298.

Sampson, C., and A. Schraeder, 2000: The Automated Tropical Cyclone Forecasting System (version 3.2). *Bull. Amer. Meteor. Soc.,* **81,** 1231–1240.

Shay, L. K., and E. W. Uhlhorn, 2008: Loop current response to Hurricanes Isidore and Lili. *Mon. Wea. Rev.,* **136,** 3248–3274.

——, G. J. Goni, and P. G. Black, 2000: Effects of a warm oceanic feature on Hurricane Opal. *Mon. Wea. Rev.,* **128,** 1366–1383.

Stephens, G. L., and Coauthors, 2002: The CloudSat mission and the A-Train: A new dimension of space-based observations of clouds and precipitation. *Bull. Amer. Meteor. Soc.,* **83,** 1771–1790.

Turk, F. J., S. DiMichele, and J. D. Hawkins, 2006: Observations of tropical cyclone structure from WindSat. *IEEE Trans. Geosci. Remote Sens.,* **44,** 645–6510.

——, J. Hawkins, K. Richardson, and M. Surratt, 2010: A tropical cyclone application for virtual globes. *Comput. Geosci.,* **37,** 13–24, doi:10.1016/j.cageo.2010.05.001.

Velden, C. S., 1989: Observational analysis of North Atlantic tropical cyclones from NOAA polar-orbiting satellite microwave data. *J. Appl. Meteor.,* **28,** 59–70.

——, T. Olander, and R. M. Zehr, 1998: Development of an objective scheme to estimate tropical cyclone intensity from digital geostationary satellite imagery. *Wea. Forecasting,* **13,** 172–186.

——, and Coauthors, 2005: Recent innovations in deriving tropospheric winds from meteorological satellites. *Bull. Amer. Meteor. Soc.,* **86,** 205–223.

——, and Coauthors, 2006: The Dvorak tropical cyclone intensity estimation technique: A satellite-based method that has endured for over 30 years. *Bull. Amer. Meteor. Soc.,* **87,** 1195–1210.